Gereon Tombrink*, Ansgar Dreier, Lasse Klingbeil and Heiner Kuhlmann

Trajectory evaluation using repeated rail-bound measurements

https://doi.org/10.1515/jag-2022-0027
Received August 12, 2022; accepted January 19, 2023;
published online February 6, 2023

Abstract: Many applications today require the precise determination of the position and orientation of a moving platform over time. However, especially in safety-critical areas, it is also important to derive quality characteristics of the trajectory estimation. This allows verification that sensors are operating within the precision and accuracy required for the application. In this paper, we propose a methodology for trajectory evaluation and address the challenges involved. Our approach is based on repeated measurements obtained using a closed loop rail track and allows the evaluation of the trajectory estimation in terms of precision and accuracy. Starting with the chronologically ordered raw data, the methodology first spatially sorts the measurements and then approximates them to a mean trajectory. The deviations between the single pose observations and the mean trajectory indicate the precision of the observed poses. With the addition of a higher-order reference, our methodology also determines the accuracy of the system under test. The applicability of our method is demonstrated by an exemplary evaluation of a low-cost inertial navigation system.

Keywords: accuracy; curve approximation; precision; quality analysis; trajectory evaluation.

1 Introduction

In many fields, the accurate determination of the position and orientation of a moving platform over time, i.e. its trajectory, is of great importance. These include, for example, the navigation of ground, air and water vehicles [1], the kinematic survey of structures such as railroad tracks [2] or kinematic laser scanning, where the quality of the point cloud depends significantly on the trajectory estimation. Especially for safety-critical applications, e.g. autonomous driving or deformation analysis, compliance with certain quality requirements, such as those described in [3] or in [4], is mandatory. To achieve this, the precision and accuracy of all six degrees of freedom of the trajectory estimation (3 DOF for position and 3 DOF for rotation) must be known. This allows the characterization of sensors concerning their quality and thus their fields of application.

However, the evaluation of the trajectory estimation proves to be challenging. This is mainly due to the kinematic nature of the measurements and the difficulty of exactly repeating them. The latter was overcome at the University of Bonn by constructing a closed loop rail track of about 140 m in length, which exhibits variations in all six degrees of freedom. An automated rail wagon is capable of repeatedly traversing the same trajectory with low mm accuracy. The system to be investigated can be mounted on this rail wagon and examined with regard to its quality.

To enable such an evaluation, we propose a methodology for the geometric quality assessment of a repeatedly recorded trajectory. Such repeated kinematic measurements along a closed loop rail track result in chronologically ordered poses that represent each lap traveled in succession. A fundamental prerequisite for the evaluation of the trajectory with respect to its precision and its accuracy is the estimation of a mean lap or trajectory. This corresponds to the approximation of spatially unorganized data. After that, we can derive the precision using the deviations between the observed poses and their mean trajectory. For accuracy analysis, we additionally need a higher-order reference trajectory to which we can compare the approximation of all laps. As long as the trajectory does not self-intersect, our methodology makes no further assumptions regarding the geometry of the trajectory. This makes it applicable to almost any repeatedly measured trajectory.

The main contribution of this paper is the development of a methodology for the evaluation of navigation sensors

***Corresponding author: Gereon Tombrink**, Institute of Geodesy and Geoinformation, University of Bonn, Nußallee 17, 53115 Bonn, Germany, E-mail: tombrink@igg.uni-bonn.de
Ansgar Dreier, **Lasse Klingbeil and Heiner Kuhlmann**, Institute of Geodesy and Geoinformation, University of Bonn, Nußallee 17, 53115 Bonn, Germany, E-mail: dreier@igg.uni-bonn.de (A. Dreier), klingbeil@igg.uni-bonn.de (L. Klingbeil), heiner.kuhlmann@uni-bonn.de (H. Kuhlmann)

using repeated kinematic measurements (Section 3). Further, we demonstrate the methodology using sensor data from a low-cost inertial navigation system (Section 4).

2 Related work

A variety of techniques for the evaluation of trajectories can already be found in the literature. This is partly because the evaluation of trajectories is relevant in many other non-geodetic fields. For example [5], study various options of comparing two trajectories in the context of a wide range of applications, such as animal migration patterns, human body movement or traffic monitoring. However, most of these methods go beyond common geodetic applications or are unsuited, especially with respect to orientations.

In the geodetic literature, the evaluation of trajectories usually focuses on kinematic positioning using GNSS. For example, Sun et al. [6] compare RTK-GNSS (Real-Time Kinematic) positions with different measurement frequencies and elevation masks in urban residential areas. The centerline of the street is used as a reference. Clausen et al. [7] investigate kinematic single-point positioning (SPP) and compare it to a reference solution computed from relative GNSS. Specht et al. [2] analyze the suitability of kinematic GNSS for surveying railroad tracks. Points determined by a total station are used as a comparison. All these publications have in common that they exclude orientations entirely and that they do not repeat the measurement or do so only to a very small extent.

Repeated kinematic GNSS measurements are performed, for example, by [3]. A rail track of 120 m in length is used, which is located on the roof of the Nottingham Geospatial Building. The total of three laps were not spatially sorted but processed in different ways and then compared point by point. The measurement took only a few minutes. Quan et al. [8] focus more on the repetition of measurements and carry out repeated kinematic GNSS measurements using a rotating arm. This is done by moving a GNSS antenna along a circular path for up to one hour. A target-tracking total station is used to create a reference with low-mm accuracy. Due to the known path geometry, the measurements do not need to be spatially sorted. A circle-fit is sufficient for the determination of the mean trajectory.

In contrast to previous work, in this paper, we propose a method that makes no assumptions about the geometry of the trajectory except that it does not self-intersect. It can handle repeated kinematic measurements of the same trajectory in multiple laps. As a result, the repeatedly measured trajectory must first be spatially sorted as a function of its arc length before it can be approximated to a mean trajectory. In the literature, there are numerous methods for reconstructing unorganized points. Ohrhallinger et al. [9] provide an overview and comparison of existing algorithms, including the approach presented in [10], which uses a minimum spanning tree (MST) for curve reconstruction. A minimum spanning tree is a cycle-free graph that connects all points while minimizing the edge length. In [11], the unorganized points are first smoothed using the so-called moving least squares (MLS) technique before selected points are approximated with quadratic B-splines. In this paper, we combine existing algorithms and adapt them to the intended geodetic application.

3 Methodology of trajectory evaluation

The aim of the methodology is a well-founded quality analysis of a trajectory repeatedly recorded in several passes. The approach is capable of examining all six degrees of freedom (x, y, z, roll, pitch, yaw) with respect to their precision and their accuracy. To enable repeated kinematic measurements, we use a closed loop rail track and refer to one pass as a lap.

The entire methodology assumes poses defined in a local coordinate frame (l-frame, see Figure 7). This is suitable for local investigations on a small scale as in the context of this work (rail track dimensions circa 63 m $\times$ 14 m). Furthermore, this simplifies the calculations because position and height can be separated directly. The origin of our l-frame lies in the mean of the measured trajectory positions while its axes are tangential to the GRS80 ellipsoid, i.e. the z-axis is perpendicular to the ellipsoid. The x-axis points to the east, the y-axis points to the north.

For both precision and accuracy assessment, a mean trajectory calculated using all individual laps is required. To obtain a mean trajectory, we first perform a spatial sorting of the data. This is illustrated in Figure 1. Consider an exemplary kinematic measurement of the same trajectory in three laps (see Figure 1a, left: cyan, blue, orange). Such measurements result in chronologically ordered data for each degree of freedom that sequentially represent each lap traversed. If we were to approximate the chronological input data directly, the approximation would also represent each individual lap rather than one single mean lap. Therefore, we need to spatially sort the measurements and represent them as a function of the arc length first (see Figure 1a, center). This allows us to approximate them to a mean trajectory (see Figure 1a, right). Figure 1b shows the same procedure for a single degree of freedom.

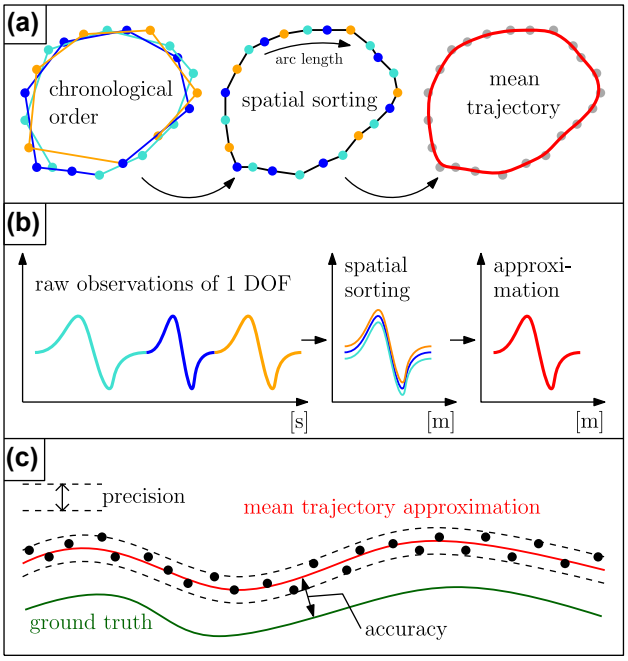

Figure 1: Overview of the developed methodology. a: Basic procedure for estimating the mean trajectory. The chronological poses are spatially sorted and then approximated. b: Isolated consideration of the same procedure for an arbitrary DOF. Spatial sorting and representation as a function of the arc length enable the approximation of all laps at once. c: Derivation of precision and accuracy based on the mean trajectory and a ground truth reference.

After spatial sorting and approximation as a function of the arc length, the comparison of individual poses with the mean trajectory then provides information about the precision or repeatability of the measurements. By comparing the mean trajectory to a reference trajectory of superior accuracy, we can draw conclusions about the accuracy of the system under investigation (see Figure 1c).

In summary, the methodology can be divided into the three central components of spatial sorting, mean trajectory approximation and the determination of quality measures. First, the spatial sorting is explained in detail in Section 3.1. Subsequently, Section 3.2 describes the approximation of the sorted data to a mean trajectory. In Section 3.3 we then derive quality measures for precision and accuracy analysis using the mean trajectory and a ground truth reference.

3.1 Spatial sorting

In our context, spatial sorting describes the sorting of unorganized poses (i.e. chronologically ordered) depending on their position along the arc length of the track. This enables the combined approximation of all laps to a single mean lap. Our approach for reconstructing the spatial sorting can be divided into smoothing (Section 3.1.1) and sorting (Section 3.1.2).

3.1.1 Smoothing using Moving-Least-Squares

Smoothing the data is a preparatory step for spatial sorting and the reconstruction of the arc length. It produces a thin curve-like point set that can be sorted substantially better than noisy data. Also, to reliably assign an arc length to each pose, a smooth point set is essential, since the arc length is reconstructed from the cumulative sum of successive positions.

To perform the smoothing of the data, we use the so-called Moving-Least-Squares (MLS) approximation. The MLS approximation was first introduced by [12] and has since been used to solve mesh-free approximation problems [11, 13, 14]. In this method, a least squares adjustment is *moved* over the set of values. Thereby, the adjustment considers only the current local neighborhood.

Let $\{\vec{\mathbf{x}}_i\}_{i\in I}$ be a set of unique data points in $\mathbb{R}^d$ and let $\{f(\vec{\mathbf{x}}_i)\}_{i\in I}$ be the corresponding function values. According to [15], the MLS approximation of degree m at point $\vec{\mathbf{x}} \in \mathbb{R}^d$ is the value $\tilde{p}(\vec{\mathbf{x}})$ at which $\tilde{p} \in \Pi_m^d$ among all $p \in \Pi_m^d$ minimizes the weighted least squares error

$$\sum_{i=1}^{N} (p(\vec{\mathbf{x}}_i) - f(\vec{\mathbf{x}}_i))^2 \cdot \theta\Big(\Big\|\vec{\mathbf{x}} - \vec{\mathbf{x}}_i\Big\|\Big). \tag{1}$$

In this context Π_m^d is the space of all polynomials of degree m in $\mathbb{R}^d$. θ is a non-negative weight function depending on the euclidean distance $\|\cdot\|$ in $\mathbb{R}^d$ and can thus be used to control the locality of the approximation.

For each position $\{\vec{\mathbf{x}}_i\}_{i\in I}$ to be approximated, a polynomial $\tilde{p}$ is fitted as best as possible to the local neighborhood of the position using a least-squares adjustment. The position is then shifted onto the approximation accordingly. For this, the MLS approximation does not require any sorting of the data, since the local neighborhood of the current point within a given radius can be efficiently determined via a distance query using a *k-d*-tree [16].

The size of the neighborhood should depend on the quality and shape of the trajectory. The noisier the data, the larger H should be chosen so that all points relevant to the current trajectory segment are considered within the MLS approximation. For complex trajectories, H should not be too large and should be chosen in combination with an appropriate polynomial degree and weight function so that characteristics of the trajectory are not lost due to smoothing. For our investigations, we can sufficiently describe the

shape of the trajectory by choosing $H = 0.05$ m, a polynomial of degree $m = 1$, i.e. a straight line in 3D, and a constant weight function within the neighborhood.

In the case of a polynomial of degree $m = 1$, the MLS approximation $\tilde{p}(\vec{\mathbf{x}})$ corresponds to the point on the 3D line that is closest to $\vec{\mathbf{x}}$ (see Figure 2):

$$\tilde{p}(\vec{\mathbf{x}}) = \vec{\mathbf{u}} + t \cdot \vec{\mathbf{r}} \tag{2}$$

with

$$t = (\vec{\mathbf{x}} - \vec{\mathbf{u}}) \cdot \vec{\mathbf{r}}. \tag{3}$$

While $\vec{\mathbf{u}}$ is the mean of the local neighborhood through which the 3D line passes, $\vec{\mathbf{r}}$ indicates the direction vector of the 3D line. Using principal component analysis (PCA), $\vec{\mathbf{r}}$ can be determined by solving an eigenvector/eigenvalue problem for the covariance matrix of the local neighborhood positions. The eigenvector corresponding to the largest eigenvalue is the sought direction vector $\vec{\mathbf{r}}$ [17].

As suggested in [11], we apply the MLS procedure iteratively. If the data is highly noisy, this allows us to smooth the data until the observations are shifted less than a specified distance.

3.1.2 Sorting using minimum-spanning-tree

Using the smoothed positions from the MLS approximation, we can determine the spatial sorting along the arc length. Applied to the raw observations of each DOF, this enables the approximation of the mean trajectory as a function of the arc length (see Figure 1b).

As proposed by [10], we use a minimum spanning tree (MST, see Figure 3) to sort the MLS approximation. The MST is a cycle-free graph that connects all points while minimizing edge lengths [18]. In our context, the shortest path connecting repeated measurements of multiple laps is one single lap that connects all positions regardless of their lap number. Thus, the MST serves exactly our intent and establishes the spatial sorting.

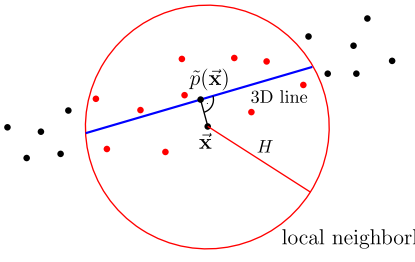

Figure 2: Calculation of the MLS approximation $\tilde{p}(\vec{\mathbf{x}})$, shown here simplified in 2D. The point $\vec{\mathbf{x}}$ is projected onto the 3D line (blue), which approximates the local neighborhood (red) as best as possible. The size of the neighborhood is defined by H.

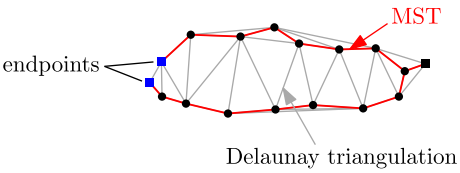

Figure 3: Minimum spanning tree applied to tube-shaped trajectories.

Since the MST is a subgraph of the Delaunay triangulation, we first construct the Delaunay triangulation of the point set [18]. The Delaunay triangulation is a meshing of a set of points using triangles. It maximizes the minimum triangle angle and exists for any point set [19]. Due to the triangulation, there are now significantly fewer possible edges between the points. As the runtime of the MST construction using Prim's algorithm depends on the number of edges, the computational cost for constructing the MST can thus be reduced significantly [20].

After constructing the MST, we can assign two endpoints to it due to the tube-like shape of the trajectory (see Figure 3, blue). This is achieved with the help of two successive breadth-first searches. Starting from any node of degree 1, i.e. with only one neighboring node (see Figure 3, squares), a breadth-first search is performed. Then, the last visited node is one of the blue endpoints. From this node, we perform another breadth-first search, which ends in the other blue endpoint and reconstructs the spatial sorting of the point set. The resulting index can be used to sort both the MLS approximation and the original observations.

It should be noted that the described methodology for sorting assumes a trajectory without self-intersections. Intersections could result in the MST not following the path that the system actually took during measurement.

After smoothing and sorting, we reconstruct the arc length by calculating the cumulative sum of the three-dimensional euclidean distances between two consecutive smoothed positions.

3.2 Mean trajectory approximation

The spatially sorted raw poses can now be approximated to a mean trajectory as a function of the arc length. Here we distinguish between the positions (Section 3.2.1) and the orientations (Section 3.2.2).

3.2.1 Position approximation

In principle, the MLS approximation described in Section 3.1 already provides an approximation of the positions.

However, in terms of evaluation, MLS lacks flexibility. An evaluation of the MLS approximation at a previously not considered location must either be done using the already calculated 3D lines, or requires a complete recalculation including the neighborhood query. Both options are suboptimal because the existing 3D lines may not be suitable for an evaluation at that given location and a recalculation of the approximation is computationally intensive.

Thus, for the approximation of the spatially sorted raw positions we apply piece-wise defined basis functions. This provides higher flexibility and enables the evaluation at any location with little effort and without the need for the original observations. The values of each DOF (x, y, z) are divided into intervals, in each of which a cubic polynomial approximates the corresponding data as best as possible (see Figure 5). After separate approximation of the x-, y- and z-component, we combine them to a three-dimensional approximation, building the foundation of positional quality analysis.

In general, the functional model for an approximation using the basis functions b_j and the parameters a_j can be formulated as follows:

$$f(x) = \sum_{j=0}^{n} a_j b_j(x). \tag{4}$$

We define $b_j(x) = x^j$ as a function of the arc length x with $n = 3$. Due to the local approach, the basis functions are only different from 0 within a fixed interval whose boundaries are described by x_S and x_E (see Figure 4). Applied to multiple intervals, this results in the situation shown in Figure 5. The measurements $\vec{\mathbf{l}}$ shown in black are divided into sections (green, blue, red). For each of these intervals, a cubic polynomial is best fitted to the data.

By introducing the following restrictions we obtain a C^1 continuous approximation:

$$\begin{aligned} f(x_E^i) &\overset{!}{=} f(x_S^{i+1}) \\ f'(x_E^i) &\overset{!}{=} f'(x_S^{i+1}). \end{aligned} \tag{5}$$

The value of the function $f(x_E^i)$ and the derivative $f'(x_E^i)$ at the end of the current interval i must therefore be

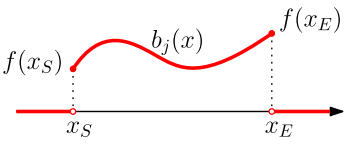

Figure 4: Basis function $b_j(x)$ for piece-wise approximation.

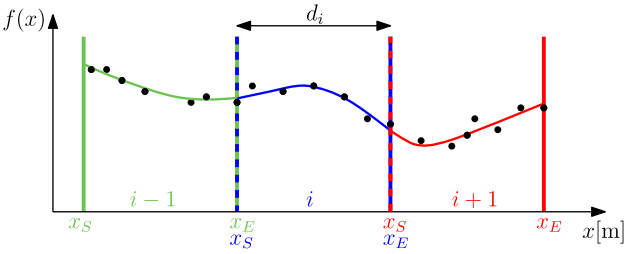

Figure 5: The set of values is divided into intervals of size d_i. Within these intervals polynomials (green, blue, red) are defined, which approximate the measured values (black) as best as possible. Continuities at interval transitions are forced by restrictions introduced during approximation.

equal to the value of the function $f(x_S^{i+1})$ and the derivative $f'(x_S^{i+1})$ at the beginning of the next interval $i+1$.

Using a least squares adjustment, the parameters $\tilde{\mathbf{p}}$ defining the polynomials as well as the estimated observations $\tilde{\vec{\mathbf{l}}}$ can be determined through Eq. (6).

$$\begin{aligned} \tilde{\mathbf{p}} &= (\mathbf{A}^T\mathbf{A})^{-1}\mathbf{A}^T\vec{\mathbf{l}} \\ \tilde{\vec{\mathbf{l}}} &= \mathbf{A}\tilde{\mathbf{p}} \end{aligned} \tag{6}$$

In this equation, $\mathbf{A}$ is the Jacobian matrix

$$\mathbf{A} = \frac{\partial f}{\partial \mathbf{p}}. \tag{7}$$

Note that the absence of a weight matrix indicates that all measurements are assumed to have the same uncertainty.

Similar to the neighborhood distance during MLS approximation, the choice of the interval size d_i (see Figure 5) should also depend on the shape and quality of the trajectory. For our investigations, we chose $d_i = 0.15$ m. To prevent the under-determination of the equation system, neighboring intervals are merged if necessary.

3.2.2 Rotation approximation

In the cubic least squares approximation described in the previous section, the distance of a raw observation from its approximation can be described by subtracting both. These differences are squared and minimized within the adjustment. Such an approach is not possible for rotations because the distance between two rotations cannot be determined by simply subtracting their Euler angles. In fact, there exist several functions for the distance between two rotations which would be suitable for our application. So, for the approximation of the rotations we have to minimize the distances between the approximation and each orientation

for one of these distance functions. Hartley et al. [21] give an overview of possible distance functions and also describes how to compute an average of multiple rotations using them. By averaging the orientations along the arc length, we obtain a rotation approximation.

In this paper, we use the so-called chordal L_2-mean, which minimizes the squared chordal distance. Reasons for this are the existence of a closed-form solution, the linear computational complexity and the ease of implementation. Given a set of n rotations q in quaternion representation, we compute the 4×4 matrix

$$\mathbf{Q} = \sum_{i=1}^{n} q_i \otimes q_i. \tag{8}$$

The eigenvector of $\mathbf{Q}$ corresponding to the maximum eigenvalue is the sought chordal L_2-mean rotation in quaternion representation [21]. This quaternion can be converted to Euler angles, if necessary.

For rotation approximation using the chordal L_2-mean, we first interpolate the rotations of all laps to the same arc lengths using Spherical Linear Interpolation (SLERP) [22] before averaging them. Due to slightly different start and end points of the individual laps, they can only be interpolated within the common range of arc lengths. Thus, there is not necessarily a mean rotation for each trajectory pose. This is illustrated exemplarily for three laps in Figure 6, in which interpolated values are marked by an empty circle and averaged rotations are displayed in red. Despite this drawback, this approach is chosen for our studies because it does not require additional parameters, such as a window width e.g. for a moving average, and the averaged rotations are always calculated from the same number of rotations.

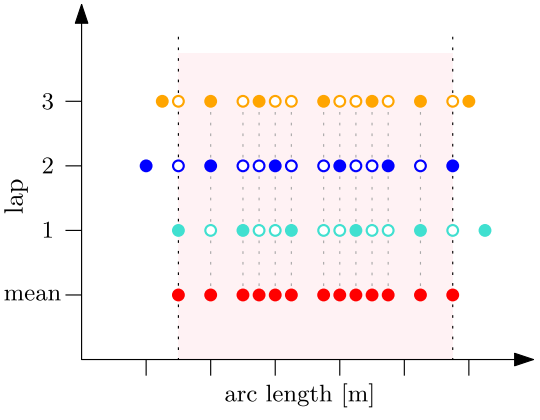

Figure 6: Averaging of the rotations using three laps as an example. The individual laps are interpolated within the common range of arc lengths (pink area). Interpolated values are depicted as an empty circle. After interpolation, the rotations can be averaged (red, "mean").

3.3 Determination of quality measures

The aim of the proposed methodology is the quality assessment of a repeatedly measured trajectory. Thereby, we focus on two quality measures, precision and accuracy. Precision describes the scattering of individual observations relative to their mean value. The accuracy specifies the deviation between the mean observation and the ground truth, usually realized by a sensor of higher accuracy.

In the following, we explain how we compute the deviations between single poses and a reference trajectory. Depending on whether a mean trajectory approximated using algorithms described in previous sections is compared to their corresponding raw observed poses or to a reference trajectory of higher accuracy, we obtain deviations indicating either precision or accuracy. As with approximation, we again distinguish between positions (Section 3.3.1) and orientations (Section 3.3.2).

Before going into detail about the computation of position and rotation deviations, we introduce two more coordinate frames, the navigation frame (n-frame) and the body frame (b-frame) (see Figure 7, blue and red).

The b-frame is a platform-fixed system, whose origin lies, for example, inside the installed inertial navigation system (INS). The coordinate axes correspond to the sensitive axes of the inertial measurement unit (IMU) which is part of the INS. For ground applications, the x-axis is usually oriented in the direction of travel, the z-axis points upwards and the y-axis points to the left relative to the direction of travel.

The n-frame is the reference frame for the orientation of the INS and has the same origin as the b-frame. Unlike the b-frame, it does not follow the platform orientation but is always oriented tangentially to the ellipsoid defined during trajectory estimation. Thus, the z-axis is always perpendicular to the ellipsoid and the x-axis points to the east while the

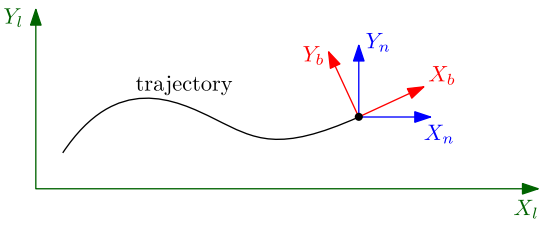

Figure 7: Simplified 2D representation of the coordinate systems involved: local frame (l-frame), navigation frame (n-frame) and body frame (b-frame).

y-axis is oriented to the north [23]. By convention, the Euler angles describe the roll, pitch and yaw of the platform with respect to the n-frame.

3.3.1 Position deviations

We would like to specify the position deviation with respect to the platform, i.e. with respect to the b-frame. This allows us to distinguish between vertical and horizontal cross-track deviations. To do this, we first construct the vector between the two positions to be compared, i.e. a single position $\vec{\mathbf{x}}_i$ and a reference position $\vec{\mathbf{x}}_r$:

$$\vec{\mathbf{d}}_\mathrm{l} = \vec{\mathbf{x}}_i - \vec{\mathbf{x}}_r. \tag{9}$$

This vector is defined in the l-frame since both compared positions are defined in the l-frame. We rotate this vector into the b-frame using

$$\vec{\mathbf{d}}_\mathrm{b} = \vec{\mathbf{d}}_\mathrm{l} \cdot \mathbf{R}_l^\mathrm{b} \tag{10}$$

in which the rotation matrix $\mathbf{R}_l^\mathrm{b}$ is composed of the three rotations about the fixed axes of the l-frame:

$$\mathbf{R}_l^\mathrm{b} = \mathbf{R}_z(\psi_A) \cdot \mathbf{R}_y(\theta_A) \cdot \mathbf{R}_x(\phi_A). \tag{11}$$

In this equation, ϕ_A, θ_A, ψ_A indicate the approximated Euler angles at the respective position.

After rotation, the desired deviations can be easily extracted from the rotated vector $\vec{\mathbf{d}}_\mathrm{b}$ and divided into horizontal and vertical cross-track deviations. The determination of an along-track deviation is not possible without further action, since there is no reference in the along-track direction.

The approach described above for calculating the position deviations assumes that orientation information is present and that both trajectories to be compared are sampled at the same points in time. These assumptions are usually not fulfilled if the trajectories of two different sensors, e.g. an INS and a total station, are to be compared. Therefore, we have also implemented an alternative approach for computing the position deviations.

In this approach, for each position to be compared to a spatially sorted reference, its two nearest neighbors A and B within the reference are determined (see Figure 8). With the help of these two neighbors, we then construct $\overrightarrow{AB}$.

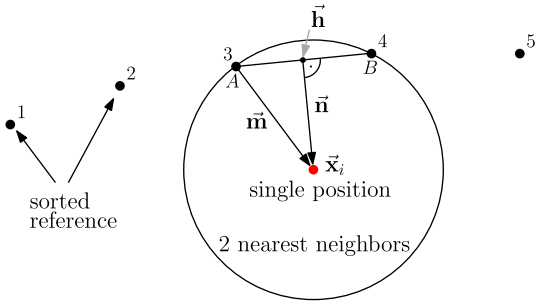

Figure 8: Computation of position deviations without orientation information (simplified in 2D).

The horizontal cross-track deviation of the single position from the reference corresponds to its 2D distance to the closest point on $\overrightarrow{AB}$, $\vec{\mathbf{h}}$, which can be obtained analogously to the MLS approximation with Eqs. (2) and (3). Thus, between two points, the reference trajectory is simplified as a straight line. The distance between two points, which can be set e.g. during the evaluation of the cubic approximation or via interpolation, should therefore be sufficiently small.

To determine the sign of the deviation, we first construct the two-dimensional vector $\vec{\mathbf{n}}$, which is perpendicular to $\overrightarrow{AB}$:

$$\vec{\mathbf{n}} = \begin{bmatrix} B_y - A_y \\ -(B_x - A_x) \end{bmatrix}. \tag{12}$$

Due to spatial sorting, $\vec{\mathbf{n}}$ always points in the same direction relative to the direction of travel. Additionally, the vector $\vec{\mathbf{m}}$ is constructed, which points from A to the single position $\vec{\mathbf{x}}_i$. Using the angle enclosed by $\vec{\mathbf{m}}$ and $\vec{\mathbf{n}}$, we can determine on which side of the line connecting A and B the single position is located. This can be reformulated as the calculation of the scalar product $k = \vec{\mathbf{m}} \cdot \vec{\mathbf{n}}$ of both vectors. If $\vec{\mathbf{x}}_i$ is located on the right relative to the direction of travel, as in the example shown in Figure 8, the enclosed angle is $\leq 90°$, resulting in a positive value for k. If the single position is located on the left, the enclosed angle $>90°$ and the scalar product k turns negative.

With this, we can specify the signed horizontal cross-track deviation:

$$-\operatorname{sign}(k) \cdot \left\| \vec{\mathbf{x}} - \vec{\mathbf{h}} \right\|. \tag{13}$$

In this equation, the sign is inverted to be consistent with the definition of the b-frame. Due to the y-axis of the b-frame pointing to the left relative to the direction of travel, left-sided deviations must have a positive sign.

The vertical cross-track deviation of $\vec{\mathbf{x}}$ corresponds to the z-component deviation between $\vec{\mathbf{x}}$ and $\vec{\mathbf{h}}$.

3.3.2 Rotation deviations

To determine the angular difference between a reference orientation and a single orientation, we need to compute the rotation from one orientation to the other. Both describe different orientations relative to the n-frame. In quaternion representation, the reference orientation can be expressed as a quaternion $\mathbf{q}^{\mathrm{n}}_{\mathrm{b}_r}$ rotating from the reference b-frame b_r to the n-frame. Analogously, we notate the single orientation as $\mathbf{q}^{\mathrm{n}}_{\mathrm{b}_i}$.

With these definitions, we can define the rotation $\mathbf{q}^{\mathrm{b}_i}_{\mathrm{b}_r}$, which rotates from the reference orientation to the single orientation:

$$\begin{aligned} \mathbf{q}^{\mathrm{b}_i}_{\mathrm{b}_r} \cdot \mathbf{q}^{\mathrm{n}}_{\mathrm{b}_r} &= \mathbf{q}^{\mathrm{n}}_{\mathrm{b}_i} \\ \mathbf{q}^{\mathrm{b}_i}_{\mathrm{b}_r} &= \mathbf{q}^{\mathrm{n}}_{\mathrm{b}_i} \cdot \mathbf{q}^{\mathrm{n}\ -1}_{\mathrm{b}_r}. \end{aligned} \tag{14}$$

Finally, we convert $\mathbf{q}^{\mathrm{b}_i}_{\mathrm{b}_r}$ to Euler angles and obtain the deviations of roll, pitch and yaw.

The approach described assumes that both orientations are available for the same location on the rail track. This is given during the comparison of the approximation with the raw observations. If different sensors are compared with each other, this requirement must be fulfilled, for example, using spherical linear interpolation as described above.

Using position and rotation deviations we can draw conclusions about the precision and the accuracy of the trajectory estimation. Thereby we distinguish between the entire measurement and individual laps.

When analyzing the precision or repeatability of the trajectory estimation, we compare the mean trajectory with the individually observed poses. For each lap, we calculate the root-mean-square error (RMS) and the bias, i.e. the mean deviation, with respect to the mean trajectory for each degree of freedom. Regarding the entire measurement, we compute the standard deviation for each DOF.

To assess the accuracy, we compare the mean trajectory with a reference trajectory of higher-order accuracy. In doing so, we calculate the mean deviation, i.e., the bias of both trajectories for each DOF.

4 Experiments

To demonstrate the viability of our methodology, we apply it to the recorded trajectory of a low-cost inertial navigation system (INS) from *SBG-Systems*. The measurement was performed using a rail track, which is part of a test environment at the University of Bonn.

The rail track was built on a campus of the University of Bonn. It is about 140 m long and has variations in all six degrees of freedom, i.e. position (3) and orientation (3) (see Figure 9). Several precisely positioned pillars are located in the vicinity of the rail track (e.g. pillar P_1, see Figure 9). They can be used to georeference target-tracking sensors such as total stations with sub-mm accuracy.

With the help of a motorized rail car, a rail wagon mounting navigation sensors can be moved automatically along the rail track (see Figure 10). This enables repeated kinematic measurements in several laps. The maximum speed of the rail car is 0.8 m/s.

For our investigations, we mounted the Ellipse2-D INS from *SBG-Systems* on the rail wagon, which is part of a kinematic laser scanning system also shown in Figure 10. In addition to a GNSS receiver, the INS features angular rate sensors, accelerometers and magnetometers for each axis. The GNSS positioning is performed with the help of two Leica AS10 antennas using Real-Time Kinematic (RTK) technology at a rate of 5 Hz. Observations from each sensor are fused at a rate of 50 Hz within an Extended Kalman Filter. The determined orientations refer to an n-frame which is tangential to the WGS84 ellipsoid.

According to the manufacturer, under good GNSS conditions and when using RTK, horizontal positioning is possible with an accuracy of 2 cm, while vertical positioning achieves an accuracy of 4 cm. Roll and pitch angles are specified with an accuracy of 0.1° and the yaw angle can be obtained with an accuracy of 0.2°. These and further specifications can be found in [24].

In addition to the system under investigation, we also attached a *Leica* GRZ122 360° prism to the wagon (see Figure 10). This prism is tracked by a *Leica* TS60 total station positioned on pillar P_1 (see Figure 9). Considering the manufacturer's accuracy specifications of 2 mm for the prism and 3 mm + 1 ppm for the continuous distance measurement of the total station, this results in a reference trajectory

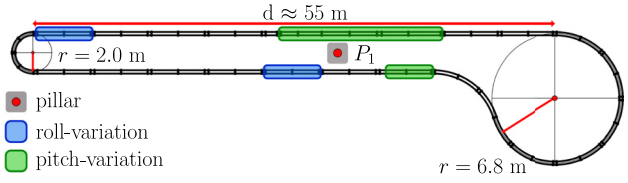

Figure 9: Rail track with a length of approx. 140 m. It features variations in the roll angle (±10°), variations in the pitch angle (±10° and ±20°) and variations in the yaw angle (±180°). In close vicinity of the rail track, there are several pillars for precise georeferencing of target-tracking sensors such as a total station.

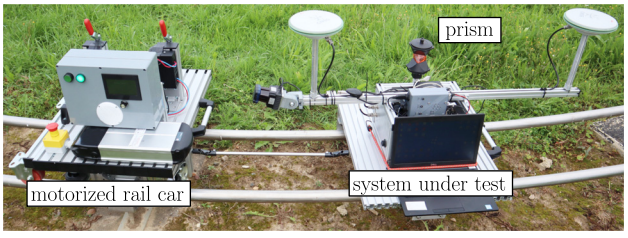

Figure 10: Motorized rail car with trailed rail wagon. The sensors under test can be mounted on the rail wagon. In addition, the rail wagon is equipped with a 360° prism, which can be tracked with a total station to generate higher-order reference trajectories.

with low mm accuracy suitable for the evaluation of RTK-GNSS based systems. In order to derive the accuracy of the system under test using this reference, its spatial relationship with respect to the prism must be known. Therefore, we determined the lever arm between both sensors, prism and INS, using a total station. Due to the lack of a reference orientation, we cannot derive the orientation accuracy with this measurement setup.

The measurement lasted almost 1 h, during which 21 laps were completed along the rail track. The total station recorded approximately 10,000 points, while the INS from *SBG-Systems* determined approximately 100,000 poses.

5 Results and discussion

In this section, we present the results of the repeated kinematic measurement using our test environment. By applying the proposed methodology, we were able to approximate the mean trajectories of the low-cost INS and the total station.

The trajectory of the total station can be used to investigate whether the rail system is able to repeat measurements precisely. The normally distributed deviations between the measured raw positions of the 360° prism and the corresponding mean trajectory (not shown in this paper) have a standard deviation of $\sigma = 1.25$ mm in horizontal and $\sigma = 0.68$ mm in vertical cross-track direction. While this verifies the repeatability of the position for our intended application, it can only verify the repeatability of the orientations to a limited extent. Rotations of the rail wagon about an axis passing through the prism could still occur unnoticed. In future investigations the repeatability of the orientations will be conclusively confirmed, e.g. with an IMU of superior accuracy.

We investigate the accuracy of the INS by comparing its mean trajectory with the mean trajectory of the total station. For analyzing the precision of the INS, we compare its mean trajectory with its raw unprocessed poses. The calculations performed within the methodology allow a wide range of investigations, which are presented here for selected examples. In addition to analyzing the quality of the system, this also allows us to verify the methodology.

5.1 Precision

Starting with the precision analysis, Figure 11 shows the deviations of the unprocessed INS trajectory from its mean trajectory in histograms. The position deviations are divided into vertical and horizontal cross-track directions (see Figure 11a). The horizontal deviations mostly scatter

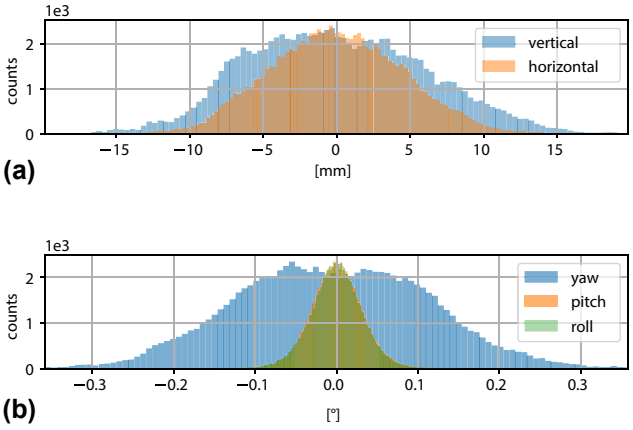

Figure 11: Histograms of the INS deviations indicating its precision. (a) Position deviations (horizontal and vertical cross-track). (b) Orientation deviations (roll, pitch, yaw).

between ±10 mm, while the vertical cross-track deviations scatter within ±15 mm. When using GNSS, the horizontal positioning is usually better than the vertical positioning as a result of the satellite geometry. Both the horizontal and vertical deviations scatter approximately normally distributed and completely within the manufacturer's specifications (horizontal 2 cm, vertical 4 cm). The standard deviation in horizontal direction is 4.51 mm, the standard deviation of the vertical cross-track deviations is about 50% higher at 6.05 mm. However, it should be noted that the horizontal deviations do not include horizontal along-track deviations and thus do not provide complete information about the precision of the horizontal positioning.

Figure 11b shows the deviations of roll, pitch and yaw. It is immediately noticeable that the deviations of the yaw angle are considerably larger than the deviations of roll and pitch. The yaw deviations are mainly between ±0.3° with a standard deviation of 0.12°, while roll and pitch both have very similar deviations between ±0.1° with a standard deviation of approximately 0.03° each. Due to the fact that the yaw angle is mainly determined by the low-cost INS using the GNSS antennas, this is plausible. Deviations within the GNSS positioning have a direct effect on the yaw angle. In contrast, roll and pitch can be determined without GNSS by using the gravity vector.

The results also show that only the roll and pitch values are within the manufacturer's specification of 0.1°, both in terms of their standard deviation and their maximum deviation. For the yaw angle, only the standard deviation is within the specification of 0.2°. In addition to measurement deviations of the INS, this could also be related to inaccuracies of the measurement setup.

Figure 12 depicts the cross-track and rotational standard deviations along the rail track. Thus, location-dependent precision anomalies in the trajectory estimation can be revealed. The vertical and horizontal cross-track deviations were combined via the L_2 norm before their standard deviation was computed. By determining the smallest rotation angle between the average orientation and the measured orientation, we can also combine the three Euler angles into a single value.

As can be seen in Figure 12a, the cross-track standard deviation is mostly in the range of 3–4 mm with occasional spikes of up to 5 mm. Thus, the magnitude is consistent with the histograms shown in Figure 11a. Higher standard deviations occur mainly in the large curve, which is located in the southeast of the rail track. The larger obstruction of the sky view, which occurs in this section of the rail track due to surrounding trees, could be responsible for this. It may be possible that a smaller number of available satellites has a negative influence on the positioning of the INS.

The standard deviation of the rotational deviations shown in Figure 12b is approximately between 0.05° and 0.15° and is mainly caused by the yaw angle (compare to Figure 11b). Increased standard deviations occur in the area of the small curve. Reasons for this could be measurement deviations or the filter algorithm of the INS. In addition, this might be an indication that the exact repeatability of the rail wagon orientation is not guaranteed in this curve.

5.2 Accuracy

To assess the accuracy of the trajectory estimation, Figure 13 shows the deviations between the mean INS trajectory and the mean reference trajectory of the total station subdivided into horizontal (Figure 13a) and vertical (Figure 13b) cross-track directions. Using the known spatial relationship of both sensors and the orientation of the rail wagon, we transformed the INS trajectory into the total station trajectory.

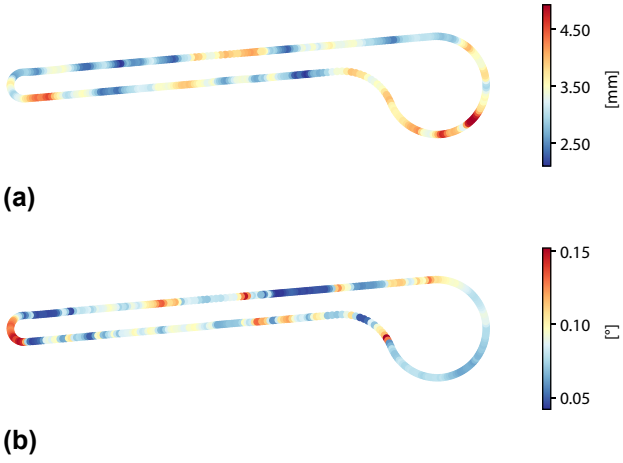

Figure 12: Cross-track and rotation standard deviations of the INS as a measure of trajectory precision. (a) Cross-track standard deviations. (b) Rotation standard deviations.

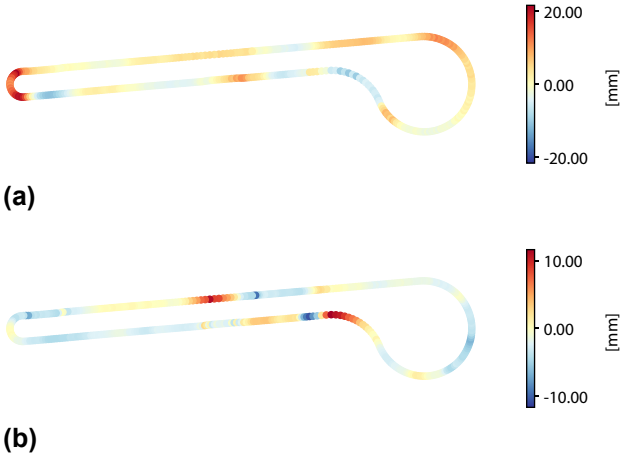

Figure 13: Bias between the mean INS trajectory and the mean reference trajectory as a measure of the accuracy of the INS trajectory. (a) Horizontal cross-track bias. (b) Vertical cross-track bias.

The bias in horizontal direction ranges mainly between −10 mm and +10 mm and shows excursions during the small curve. On average, the trajectory of the INS deviates +1.76 mm from the total station trajectory in horizontal direction. The bias in the vertical direction mostly exhibits values smaller than ±5 mm with a mean deviation of −1.36 mm.

The magnitudes of the deviations show a clear correlation with the characteristics of the rail track. Large deviations in the horizontal direction occur mainly in the small curve, while an increased bias in the vertical direction is found in sloping areas of the rail track. Possible reasons for this are an inaccurate position and/or orientation determination of the INS, or deviations of the rail wagon. Furthermore, a recurring sequence of positive and negative values along the track is noticeable, especially in the horizontal bias (Figure 13a). This could be related to systematic deviations of the 360° prism [25].

Regardless of the increased bias in some regions of the rail track, the determined deviations are well within the expectations for the accuracy of RTK-GNSS based positioning systems. Because no reference orientation is available, we can only investigate positioning in terms of accuracy. However, the orientations of the INS are indirectly involved in this process as a result of the transformation of the INS trajectory.

6 Conclusion and future work

In this paper, we presented a novel approach to evaluate navigation sensors using repeated kinematic measurements. The methodology allows the determination of precision and accuracy for all six degrees of freedom, i.e. position (x, y, z) and orientation (roll, pitch, yaw), and can be applied to arbitrary trajectories that do not self-intersect. Due to the repetition, the chronologically measured poses have to be spatially sorted first. In a second step, they are approximated, which enables the geometric quality analysis of the trajectory. Depending on whether the trajectory is compared to its own approximation or to a higher-order reference trajectory, we can determine either the precision or the accuracy of the trajectory.

The presented methodology was successfully applied to a data set of a low-cost inertial navigation system (INS). This allowed both the verification of the methodology and the evaluation of the low-cost INS. Using the methodology, we were able to assess the quality of the system either in a location-dependent manner, divided into laps, or holistically. Both in terms of precision and accuracy, the system complies with the manufacturer's specifications. Thus, the results are plausible and therefore confirm the correct operation of the INS and the developed methodology.

In future work, the methodology could be extended by also enabling the determination of along-track deviations. This would require a reference in along-track direction. Further investigation is also needed for obtaining an orientation accuracy. Due to the difficulty of creating a reference orientation, alternative approaches may need to be considered.

Author contributions: All the authors have accepted responsibility for the entire content of this submitted manuscript and approved submission.

Research funding: This work was partly funded by the Deutsche Forschungsgemeinschaft (DFG, German Research Foundation) under Germany's Excellence Strategy–EXC 2070–390732324. Moreover, the study is partially funded by the German Federal Ministry of Education and Research (BMBF) in the framework MTI "Mensch Technik Interaktion" (grant no. 16SV8575).

Conflict of interest statement: The authors declare no conflicts of interest regarding this article.

References

1. Teunissen PJG, Montenbruck O. Springer handbook of global navigation satellite systems. Springer handbooks, 1st ed. Cham, Switzerland: Springer; 2017.
2. Specht C, Wilk A, Koc W, Karwowski K, Dąbrowski P, Specht M, et al. Verification of GNSS measurements of the railway track using standard techniques for determining coordinates. Rem Sens 2020;12:2874.
3. Stephenson S, Meng X, Moore T, Baxendale A, Edwards T. Precision of network real time kinematic positioning for intelligent transport systems. In: European navigation conference. Toulouse, France; 2011.
4. Olsen MJ, Roe GV, Glennie C, Persi F, Reedy M, Hurwitz D, et al. Guidelines for the use of mobile LIDAR in transportation applications. Washington, DC, USA: TRB; 2013, TRB NCHRP Final Report 748.
5. Su H, Liu S, Zheng B, Zhou X, Zheng K. A survey of trajectory distance measures and performance evaluation. VLDB J 2020;29:3—32.
6. Sun QC, Xia JC, Foster J, Falkmer T, Lee H. Pursuing precise vehicle movement trajectory in UrbanResidential area using multi-GNSS RTK tracking. Transport Res Procedia 2017;25:2356—72.
7. Clausen P, Gilliéron PY, Perakis H, Gikas V, Spyropoulou I. Positioning accuracy of vehicle trajectories for road applications. In Proceedings of the 22nd ITS World Congress, Bordeaux, France; 2015.
8. Quan Y, Lau L. Development of a trajectory constrained rotating arm rig for testing GNSS kinematic positioning. Measurement 2019;140:479—85.
9. Ohrhallinger S, Peethambaran J, Parakkat AD, Dey TK, Muthuganapathy R. 2D points curve reconstruction survey and benchmark. Comput Graph Forum 2021;40:611—32.
10. De Figueiredo LH, de Miranda Gomes J. Computational morphology of curves. Vis Comput 1994;11:105—12.
11. Lee IK. Curve reconstruction from unorganized points. Comput Aided Geom Des 2000;17:161—77.
12. McLain DH. Drawing contours from arbitrary data points. Comput J 1974;17:318—24.
13. Lancaster P, Salkauskas K. Surfaces generated by moving least squares methods. Math Comput 1981;37:141—58.
14. Levin D. Mesh-independent surface interpolation. In: Geometric modeling for scientific visualization. Berlin, Heidelberg: Springer; 2004:37—49 pp.
15. Levin D. The approximation power of moving least-squares. Math Comput 1998;67:1517—31.
16. Bentley JL. Multidimensional binary search trees used for associative searching. Commun ACM 1975;18:509—17.
17. Förstner W, Wrobel BP. Photogrammetric computer vision. Schweiz: Springer International Publishing; 2016.
18. de Berg M, Cheong O, van Kreveld M, Overmars M. Computational geometry, 3rd ed. Berlin, Heidelberg: Springer; 2008.
19. Cheng SW, Dey TK, Shewchuk J, Sahni S. Delaunay mesh generation. Boca Raton: CRC Press; 2013.
20. Prim RC. Shortest connection networks and some generalizations. Bell Syst Tech J 1957;36:1389—401.

21. Hartley R, Trumpf J, Dai Y, Li H. Rotation averaging. Int J Comput Vis 2013;103:267—305.
22. Shoemake K. Animating rotation with quaternion curves. In: SIGGRAPH '85: proceedings of the 12th annual conference on computer graphics and interactive techniques. San Francisco: ACM; 1985:245—54 pp.
23. Kuhlmann H, Klingbeil L. Ingenieurgeodäsie: Handbuch der Geodäsie, herausgegeben von Willi Freeden und Reiner Rummel, chapter mobile Multisensorsysteme, 1st ed. Berlin, Heidelberg: Springer Spektrum; 2015:1—36 pp.
24. SBG-Systems. ELLIPSE 2 AHRS & INS hardware manual; 2017. Available from: https://www.sbg-systems.com.
25. Lackner S, Lienhart W. Impact of prism type and prism orientation on the accuracy of automated total station measurements. In: Proc. 3rd joint international symposium on deformation monitoring. Vienna; 2016.